Boundary Currents and Watermass Transformation in Marginal Seas[*]

MICHAEL A. SPALL

Department of Physical Oceanography, Woods Hole Oceanographic Institution, Woods Hole, Massachusetts

ABSTRACT

The properties of watermass transformation and the thermohaline circulation in marginal seas with topography and subject to a spatially uniform net surface cooling are discussed. The net heat loss within the marginal sea is ultimately balanced by lateral advection from the open ocean in a narrow boundary current that flows cyclonically around the basin. Heat loss in the interior is offset by lateral eddy fluxes originating in the boundary current. The objectives of this study are to understand better what controls the density of waters formed within the marginal sea, the temperature of the outflowing waters, the amount of downwelling, and the mechanisms of heat transport within the marginal sea. The approach combines heat budgets with linear stability theory for a baroclinic flow over a sloping bottom to provide simple theoretical estimates of each of these quantities in terms of the basic parameters of the system. The theory compares well to a series of eddy-resolving primitive equation model calculations. The downwelling is concentrated within the boundary current in both a diffusive boundary layer near topography and an eddy-driven region on the offshore edge of the boundary current. For most high-latitude regions, the horizontal gyre is expected to transport more heat than does the overturning gyre.

1. Introduction

Marginal seas are often regions of net buoyancy loss as a result of either cooling or evaporation and, because of their semienclosed geometry, are regions of formation of dense intermediate or bottom waters. These waters generally have quite distinct water mass properties relative to the open ocean and make a significant contribution to the global thermohaline circulation through the transport of heat and salt. They also influence the large-scale circulation throughout the water column because they have anomalously low potential vorticity. Understanding what controls the formation rate and properties of such water masses is an important part of understanding the global oceanic thermohaline circulation. In this context, marginal seas can be relatively small geographically, such as the Red Sea or the Adriatic Sea, or they can be of planetary scale, such as the Mediterranean Sea or the Nordic seas. The important characteristic for the present study is that the marginal sea is a semienclosed basin that is subject to a net buoyancy loss.

The areas of deepest convection in marginal seas are generally localized to regions with spatial scales $O(100$ km). The properties of waters formed by such localized deep convection have received much recent attention. Idealized numerical and laboratory experiments have shown that lateral fluxes out of localized deep convection sites by mesoscale eddies can balance surface buoyancy fluxes (Visbeck et al. 1996, hereinafter VMJ; Marshall and Schott 1999 and the references therein). By making use of stability theory, the properties (density, depth) of deep convection sites in interior regions of the ocean subject to localized surface fluxes can be estimated with some success (VMJ; Marshall and Schott 1999; Chapman 1998). These results demonstrate that lateral heat fluxes due to mesoscale eddies can play a central role in controlling the properties of the large-scale thermohaline circulation.

While compelling, these studies make several rather restrictive assumptions when compared with the actual problem of buoyancy loss in a marginal sea. They have generally been formulated with a net buoyancy loss that is localized in the interior of the basin, often with an abrupt transition in its strength. Chapman (1998) allowed for a gradual transition in the surface forcing strength and found that the equilibrium properties had a different scaling, most notably with regard to the Coriolis parameter. On the other hand, atmospheric forcing varies on spatial scales much larger than the oceanic deformation radius (ice edge effects and polynyas are a notable exception) and is often nonzero over much or most of the marginal seas. The net heat flux out of the ocean in these studies has also made it impossible to

Corresponding author address: Dr. Mike Spall, Woods Hole Oceanographic Institution, 360 Woods Hole Rd., MS 21, Woods Hole, MA 02543.
E-mail: mspall@whoi.edu

obtain equilibrium solutions. Last, although it has been shown that the net vertical motions in interior regions of buoyancy loss are not significantly different from zero, it is well known that marginal seas do experience a net downward flux of water. Theoretical arguments favor near-boundary regions for the net downwelling to take place (Spall 2003; Pedlosky 2003; Spall and Pickart 2001), an aspect not considered in the previous open-ocean configurations.

For marginal seas connected to the open ocean through a narrow strait, the net buoyancy flux at the ocean's surface must be balanced by lateral advection through the strait. This requires both lateral boundaries and a reservoir of buoyant water. Lateral advection also appears to be important for less geographically constrained regions of buoyancy loss such as the Nordic seas (Mauritzen 1996) and the Labrador Sea (Katsman et al. 2004; Lilly et al. 2003; Straneo 2004, manuscript submitted to *J. Phys. Oceanogr.*). Understanding the interaction between the narrow boundary currents that are required to balance the net buoyancy flux and the vast interior regions over which there are significant surface fluxes is key to understanding the heat budget in marginal seas and, hence, the overall process that controls water mass transformation.

In a recent study, Walin et al. (2003, unpublished manuscript, hereinafter WBNO) explore the influence of cooling in a marginal sea on the structure of the resulting boundary currents. Their interest was on the transformation of a baroclinic inflowing boundary current into a barotropic outflowing boundary current. The heat loss was concentrated in the boundary current, and was strong in the sense that the baroclinicity of the inflowing boundary current was entirely eroded before it encircled the marginal sea. The forcing was designed such that there was little cooling of the interior of the marginal sea, and so the exchange between the boundary current and the interior was weak. The circulations investigated in the present paper are complementary in that the outflowing currents are (generally, but not always) baroclinic and the heat loss in the interior of the marginal sea is significant.

Numerous studies have been successful in relating the basin-scale buoyancy-forced overturning circulation and meridional heat transport to the basic parameters of the system; a recent review is given by Park and Bryan (2000). These studies differ from the current one in several important ways. Primarily, they are aimed at the large-scale overturning circulation and assume that all of the downwelling at high latitudes is balanced by a diapycnal upwelling at mid- and low latitudes. The present study makes no assumptions about where the waters upwell, or what dynamics are active in the upwelling region. For example, the upwelling could take place via diapycnal mixing of density in the midlatitude deep ocean or it could take place within the surface mixed layer where the isopycnals outcrop at high latitudes. In addition, previous studies generally did not properly re-

solve the mesoscale eddies either because of low resolution in models (e.g., Bryan 1987; Park and Bryan 2000; Spall and Pickart 2001) or, in the case of laboratory experiments, the deformation radius was the same scale as the basin (e.g., Park and Whitehead 1999). The temperature anomaly of the deep waters (required to estimate heat transport and advective speeds) is specified or diagnosed in these previous studies, while it is predicted as part of the solution in the current study.

The objective of this work is to understand better what controls the properties of water mass transformation and thermohaline circulation in marginal seas subject to buoyancy loss. The basic circulation characteristics are first described using an eddy-resolving general circulation model. Theoretical arguments are then used to estimate the parameter dependencies of the density of water formed in the marginal sea, the density of the water flowing out of the marginal sea, the amount of downwelling within the marginal sea, and the relative importance of horizontal versus vertical gyres in the heat transport within the marginal sea. The theory compares well to results from a series of numerical model calculations.

2. Thermohaline circulation in an idealized marginal sea

The thermohaline circulation in an idealized semienclosed marginal sea will first be explored using the Massachusetts Institute of Technology (MIT) primitive equation numerical model (Marshall et al. 1997). The model solves the momentum and density equations using level (depth) coordinates in the vertical and a staggered C grid in the horizontal. The model retains a free surface. A linear equation of state is used so that density is proportional to temperature as $\rho = \rho_0 - \alpha(T - T_b)$, where ρ_0 is a reference density for seawater, $T_b = 4°C$ is the initial temperature at the bottom, and the thermal expansion coefficient $\alpha = 0.2$ kg m^{-3} °C^{-1}. The model is initialized at rest with a uniform stratification such that $T_0(z) = T_b + T_z(z_b - z)$, with the maximum bottom depth $z_b = 1000$ m and vertical gradient $T_z = 1.5 \times 10^{-3}$ °C m^{-1} ($N^2 = 3 \times 10^{-6}$ s^{-1}), although the results have not been found to be very sensitive to this initial stratification. The initial temperature at the uppermost model level (50 m) is 5.35°C. The model is configured with uniform horizontal grid spacing of 5 km and 10 levels in the vertical, each with thickness 100 m. This vertical resolution does not resolve the bottom Ekman layer but does resolve the first baroclinic mode and, with the partial cell treatment of bottom topography, the topography slope. However, for small Ekman numbers, the growth rate of the most unstable waves, which is the primary physical process of interest here, are not significantly affected by the bottom Ekman layer (Stipa 2003, manuscript submitted to *Geophys. Astrophys. Fluid Dyn.*, hereinafter SGAFD). The Coriolis parameter is 10^{-4} s^{-1} and constant so that the internal deformation
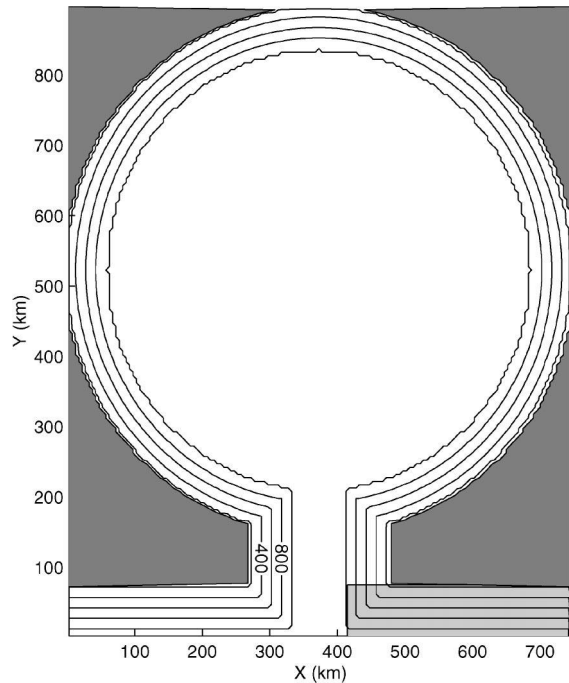
FIG. 1. Basin configuration and bottom topography (contour interval 200 m). The lightly shaded region in the lower right is where the model temperature is restored toward a uniform stratification with time scale 50 days.

offshore of the boundary, giving a bottom slope of h_r = 1.33×10^{-2} (see Table 1). Parameter sensitivity studies that are carried out in the following section will mostly use a smaller basin of 500-km diameter (for computational efficiency); however, the basic circulation and governing physics are similar to the larger basin. The temperature within the lightly shaded region of the open ocean is restored toward the initial uniform stratification $T_0(z)$ with a time scale of 50 days. In this way, the properties of the water flowing into the marginal sea are essentially fixed, independent of what processes take place in the marginal sea. The exchange rate through the strait is not specified, but rather emerges as part of the solution. The model is forced by an annual cycle of cooling of strength 120 W m^{-2} applied over the entire marginal sea for 2 months followed by no forcing for 10 months (annual mean heat loss is 20 W m^{-2}). This annual cycle is repeated for an interval of 25 years. The sensitivity of the water mass transformation and circulation to changes in the basin size and depth, bottom slope and width, strength of forcing, and Coriolis parameter will be explored in the following section.

Subgrid-scale processes are parameterized using Laplacian viscosity and diffusion in both horizontal and vertical directions. Lateral boundary conditions are no slip and there is no heat flux through the solid boundaries. The horizontal diffusivity is 30 m² s^{-1} and the horizontal viscosity is 50 m² s^{-1}. The vertical diffusion coefficient is 10^{-5} m² s^{-1}, while the vertical viscosity coefficient is 2×10^{-4} m² s^{-1}. The bulk characteristics of the watermass transformation in the marginal sea are not overly sensitive to these choices, provided that the model dissipation is not so strong that it suppresses the instability of the boundary current. The subgrid-scale mixing can, however, influence the details of the down-

radius based on this open-ocean stratification is approximately 17 km and well resolved by the horizontal grid.

The model domain for the central calculation consists of a circular basin 750 km in diameter connected to an "open ocean" through a channel 200 km wide (Fig. 1). The bottom slopes downward from 200-m depth on the outer boundary to 1000-m depth at a distance 60 km

TABLE 1. Model run parameters, units: radius (km); f_0 (s^{-1}); Q (W m^{-2}); L (km); h_r dimensionless; depth (m); $T_{in}-T_0$ (°C); downwelling (10^6 m³ s^{-1}), and symbols used in Fig. 12.

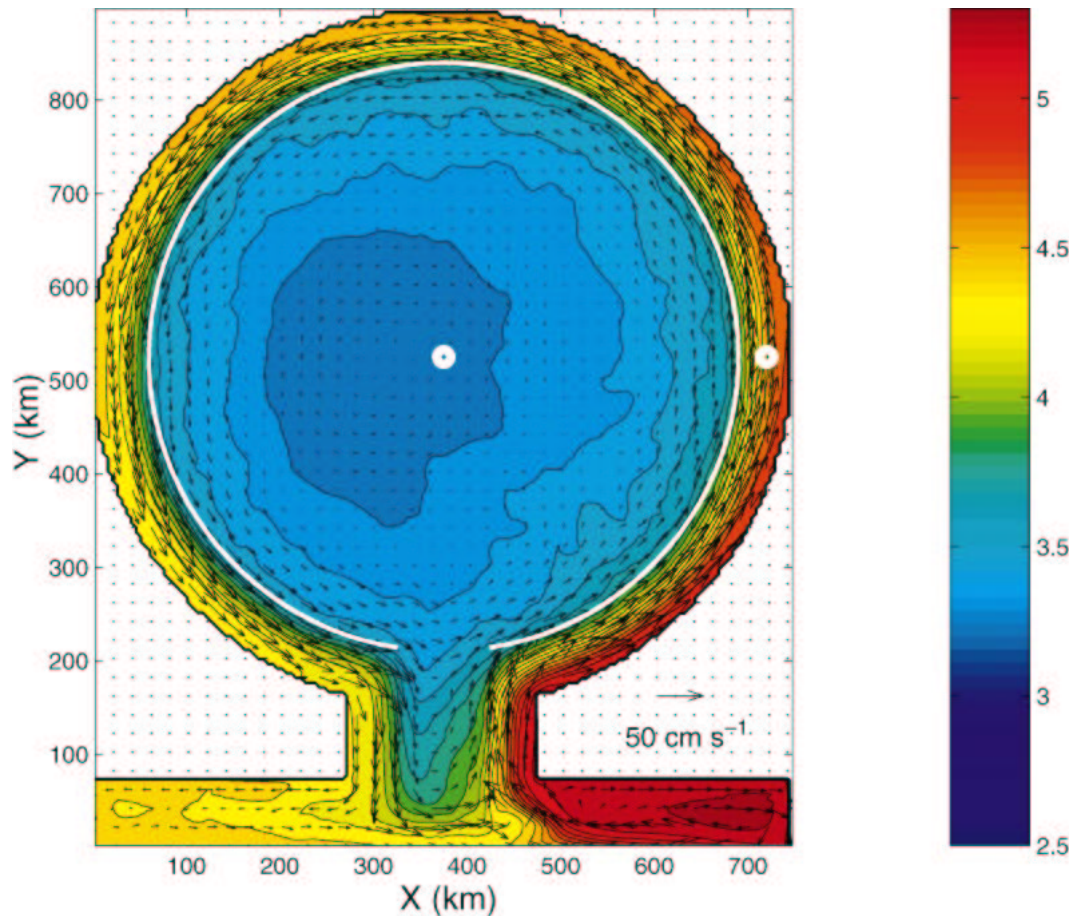| Run	Radius	f_0	Q	L	h_r	Depth	$T_{in}-T_0$	Downwelling	Symbol
1	375	1×10^{-4}	20	60	0.0133	1000	1.62	0.59	square
2	250	1×10^{-4}	20	60	0.0133	1000	1.15	0.28	asterisk
3	185	1×10^{-4}	20	60	0.0133	1000	0.93	0.19	square
4	250	1×10^{-4}	20	60	0.0067	1000	0.97	0.50	triangle
5	250	1×10^{-4}	20	60	0.0033	1000	0.83	0.59	triangle
6	250	1×10^{-4}	20	60	0.0	1000	0.55	0.76	star
7	250	1×10^{-4}	10	60	0.0133	1000	0.81	0.23	circle
8	250	1×10^{-4}	40	60	0.0133	1000	1.69	0.42	circle
9	250	1×10^{-4}	60	60	0.0133	1000	2.05	0.47	circle
10	250	0.25×10^{-4}	20	60	0.0133	1000	0.92	0.90	diamond
11	250	0.5×10^{-4}	20	60	0.0133	1000	0.94	0.49	diamond
12	250	2×10^{-4}	20	60	0.0133	1000	1.39	0.16	diamond
13	250	3×10^{-4}	20	60	0.0133	1000	1.79	0.11	diamond
14	250	1×10^{-4}	20	30	0.0266	1000	1.06	0.60	plus sign
15	250	1×10^{-4}	20	100	0.008	1000	1.12	0.18	plus sign
16	250	1×10^{-4}	20	60	0.0067	500	2.05	0.14	triangle (down)
17	250	1×10^{-4}	20	60	0.0267	2000	0.67	0.57	triangle (down)
18	375	1×10^{-4}	40	60	0.0133	1000	1.99	0.80	cross
19	250	1×10^{-4}	20	30	0.0067	1000	0.82	0.65	triangle (left)

FIG. 2. Mean upper-level temperature and horizontal velocity (every fourth grid point) for the central calculation (contour interval = 0.1°C). Locations of the time series in Fig. 3 are indicated by the white circles; the boundary between the sloping topography and the flat interior is indicated by the white line.

welling boundary layer near the sidewalls, particularly when the bottom is flat (Spall 2003). The weaker sensitivity found here may be a result of the bottom topography. The width of the boundary current over a sloping bottom is controlled by the width of the topography, whereas it scales as the internal deformation radius times the square root of the Prandtl number for a flat bottom (Spall 2003). At high latitudes, where cooling is active, the topographic slope is generally much wider than the deformation radius, and so frictional boundary layers are likely to be much weaker than in Spall (2003). A similar lack of sensitivity to subgrid-scale mixing was also found in the calculations with a sloping bottom by WBNO.

This configuration and forcing differ from most previous studies of localized cooling in several important ways. First, the marginal sea is connected to an open ocean, as in Spall (2003) and WBNO, so that the heat loss in the marginal sea can be balanced by an advective flux through the strait and equilibrium solutions can be obtained. Unlike Spall (2003), however, the cooling is (more realistically) applied over the entire marginal sea.

This does not introduce an artificially small length scale into the problem that arises when the cooling is confined to a localized region of the ocean. Any spatial variability that arises in the solutions is a result of lateral advection in the ocean. The second difference from previous studies, except that of WBNO, is that the bottom topography is sloped near the boundaries. This allows for the development of strong boundary currents and, as will be shown, plays a fundamental role in the properties of the water mass transformation in the marginal sea.

The model has been integrated until a statistical equilibrium is achieved. The mean temperature and horizontal velocity at 50-m depth averaged over the final 5 years of a 25-yr simulation are shown in Fig. 2. The white line marks the region where the topography becomes flat in the interior. The coldest waters are found in the interior of the marginal sea, where there are domed isopycnals and a weak anticyclonic circulation. There is also a strong, warm boundary current flowing cyclonically around the basin. The maximum mean velocity in the boundary current is approximately 25 cm s^{-1}. The temperature of the boundary current decreases
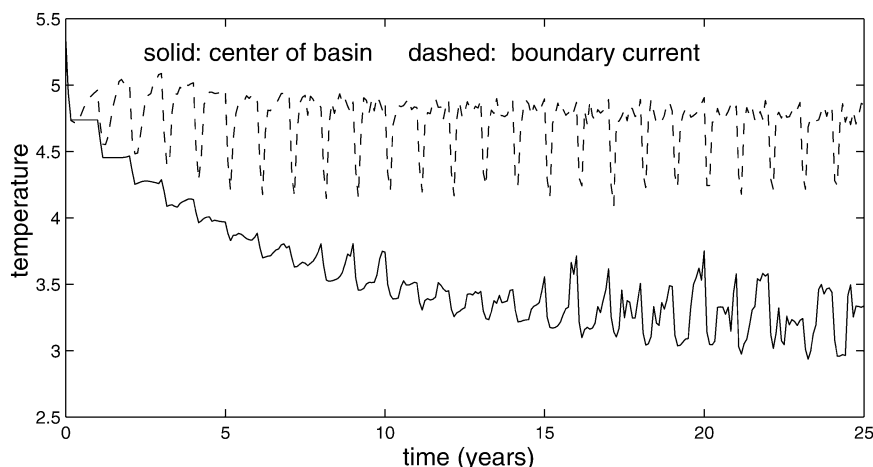
FIG. 3. Time series of temperature (°C) at the center of the basin (solid line) and in the boundary current (dashed line); see Fig. 2 for locations.

monotonically as it flows around the basin such that the outflowing water is colder than the inflowing water. It is this decrease in temperature within the boundary current that balances the net heat loss due to atmospheric forcing within the marginal sea.

Time series of the temperature at 50-m depth at the midpoint of the marginal sea and within the boundary current ($x = 725$ km, $y = 525$ km; locations are indicated by the white circles in Fig. 2) are shown in Fig. 3. The boundary current settles down to a fairly regular seasonal cycle very quickly, within a few years. The temperature drops rapidly when the surface cooling is applied and, because of lateral advection from the open ocean, rebounds to approximately 4.8°C after cooling ceases. The temperature in the interior takes much longer, approximately 15 years, to arrive at an equilibrium seasonal cycle. At equilibrium, the seasonal variation in sea surface temperature is $O(0.5°C)$. The warming in summer is provided by eddies transporting heat from the warm boundary current into the interior. Because this restratification mechanism is not effective early in the calculation, the water initially cools year after year. Once the temperature contrast between the interior and the boundary current is sufficiently strong, eddies formed from the boundary current transport warm water into the interior to balance heat loss at the surface. This balance is similar to what has been found for localized cooling over a flat bottom in a stratified ocean by VMJ, Chapman (1998), and Marshall and Schott (1999). In those cases, however, the instabilities arise from a geostrophic rim current that forms around the region of localized cooling, not from a boundary current that encircles the basin.

The mean vertical structure in the marginal sea is indicated by zonal sections at $y = 525$ km shown in Fig. 4. The interior is filled with cold, low-potential-vorticity water. There is increased potential vorticity near the surface as a result of weak stratification, and

the gently sloping isopycnals are balanced by a weak cyclonic shear $O(1$ cm s$^{-1})$. The circulation in the interior is anticyclonic, however, in opposite sense to the boundary current circulation. The boundary region is characterized by a warm, strong, surface-intensified cyclonic boundary current with horizontal velocities in excess of 20 cm s^{-1}. The stratification is also strong in the upper 200–300 m of the boundary current (the small-scale temperature and potential vorticity anomalies very near the bottom are an artifact of the contouring routine and the definition of bottom topography in the model; they are not active in the flow). The southward-flowing waters along the western boundary are colder, and have slower maximum velocity and slightly deeper vertical structure, than the northward-flowing waters on the eastern boundary.

The restratification of the interior of the marginal sea is indicated by the average seasonal temperature profile (average month 1, month 2, etc.) within the central 50 km of the basin calculated over the final 5 years of integration in Fig. 5. At the beginning of the year the interior is stratified with warm water in the upper few hundred meters. This stratification is eroded through the 2-month cooling period so that at the beginning of month 3 the central region of the marginal sea is very cold and unstratified. Within 2 months after cooling has ceased the upper ocean begins to restratify, as indicated by the arrival of warmer waters by the middle of month 4. The later arrival of warm, stratified waters throughout the model summer provides the majority of the restratification in the interior.

The initial, weak restratification results from waters in the interior of the marginal sea that were not fully convected during the winter. Figure 6 shows the instantaneous temperature at 50-m depth at the end of the cooling period in year 22. The surface waters are cold throughout the interior, but there are weak lateral variations. The initial restratification in Fig. 5 is provided
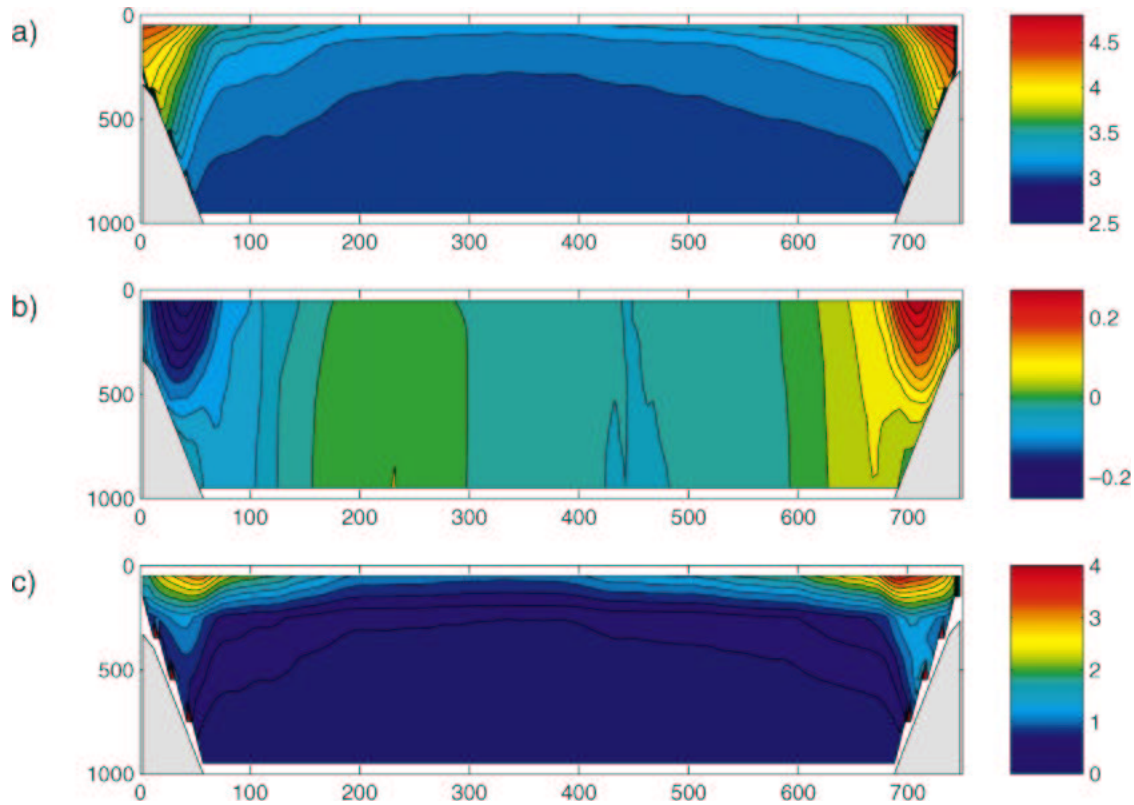
FIG. 4. Mean zonal sections through the midlatitude of the basin: (a) temperature (°C), (b) meridional velocity (m s^{-1}), and (c) potential vorticity.

by the large-scale remnants of warmer waters in the interior remaining from the previous year. The scale of these features is much larger than the internal deformation radius and they do not result from baroclinic instability of the deep convection site during this winter. This is consistent with the observational findings of Lilly et al. (1999) that deep convection is patchy on spatial scales $O(100 \text{ km})$ in winter in the Labrador Sea. Smaller,

deformation-scale features are also beginning to penetrate into the interior that do result from instabilities along the offshore edge of the boundary current.

This lateral variation in stratification is also indicated in Fig. 7 by the mixed layer depth at the end of winter. There is deep mixing throughout most of the interior of the marginal sea, but the slightly warmer areas over the flat interior remain weakly stratified at the end of winter.
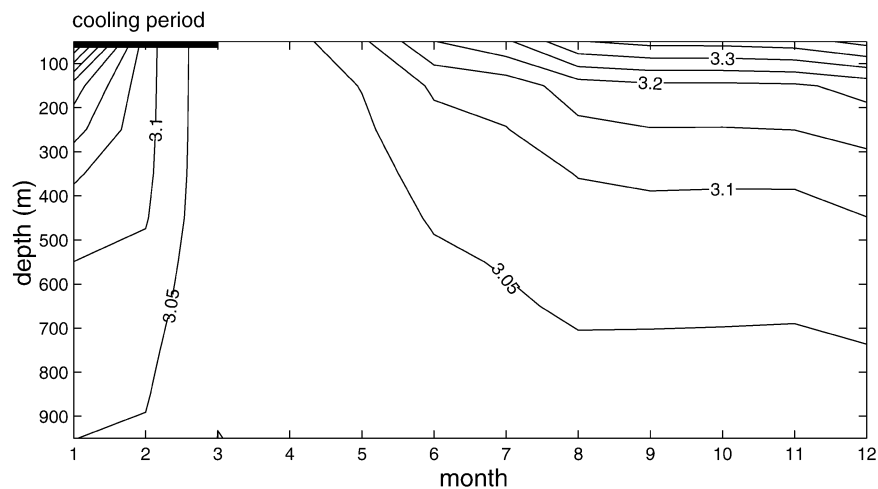

FIG. 5. Average seasonal profile of temperature (°C) within the central 50 km of the basin.

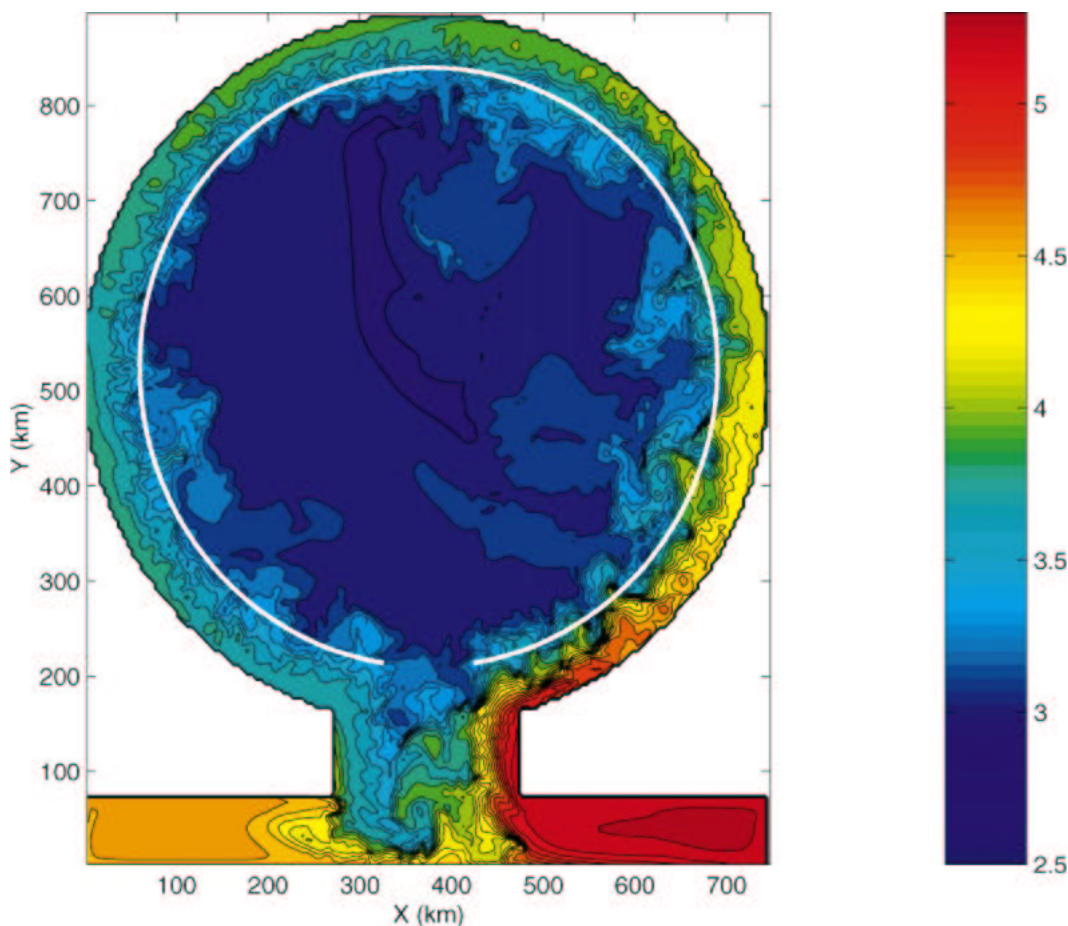FIG. 6. Upper-level temperature (°C) at the end of the cooling period in year 22; contour interval = 0.1.

It is these waters that result in the rapid, weak restratification in Fig. 5. Such remnants of the previous summer stratification are generally found at the end of winter, although the amount varies from year to year.

The later, stronger restratification results from eddies formed from the boundary current during spring and summer months when the waters are warmer and more stratified. Figure 8 shows the 50-m temperature at the end of month 4. Lateral advection from the open ocean has warmed the boundary current over most of the basin. Filaments and eddies originating from the offshore edge of the boundary current extend into the interior. They are not characterized by pinched-off rings resulting from very large meanders, such as is often found along the Gulf Stream, for example. There is a turbulent cascade such that the length scale of the perturbations grows from the deformation scale at their source near the offshore edge of the boundary current in late winter to $O(100 \text{ km})$ in the interior at the end of summer. It is this cascade of scales that results in the large regions of warmer, weakly stratified waters at the end of winter seen in Figs. 6 and 7. The mixed layer depth is shallow over most of the basin at this time (not shown).

3. Heat balances and residual circulation

The balance of terms in the heat equation is useful to elucidate the means by which heat is redistributed within the marginal sea. The temperature equation solved by the MIT primitive equation model is written as

$$\frac{\partial T}{\partial t} = -\boldsymbol{\nabla} \cdot (\mathbf{v}T) - \frac{\partial(wT)}{\partial z} + A_T \nabla^2 T + K_T \frac{\partial^2 T}{\partial z^2}, \quad (1)$$

where $\mathbf{v} = u\mathbf{i} + v\mathbf{j}$ is the horizontal velocity vector. The advection terms [first and second on the right-hand side of (1)] are further decomposed into mean and eddy components:

$$\boldsymbol{\nabla} \cdot (\mathbf{v}T) + \frac{\partial(wT)}{\partial z} = \boldsymbol{\nabla} \cdot (\overline{\mathbf{v}'T'}) + \frac{\partial(\overline{w'T'})}{\partial z}$$

$$+ \boldsymbol{\nabla} \cdot (\overline{\mathbf{v}}\,\overline{T}) + \frac{\partial(\overline{w}\,\overline{T})}{\partial z}, \quad (2)$$

where the overbars denote a time average and primes are deviations from the time mean.

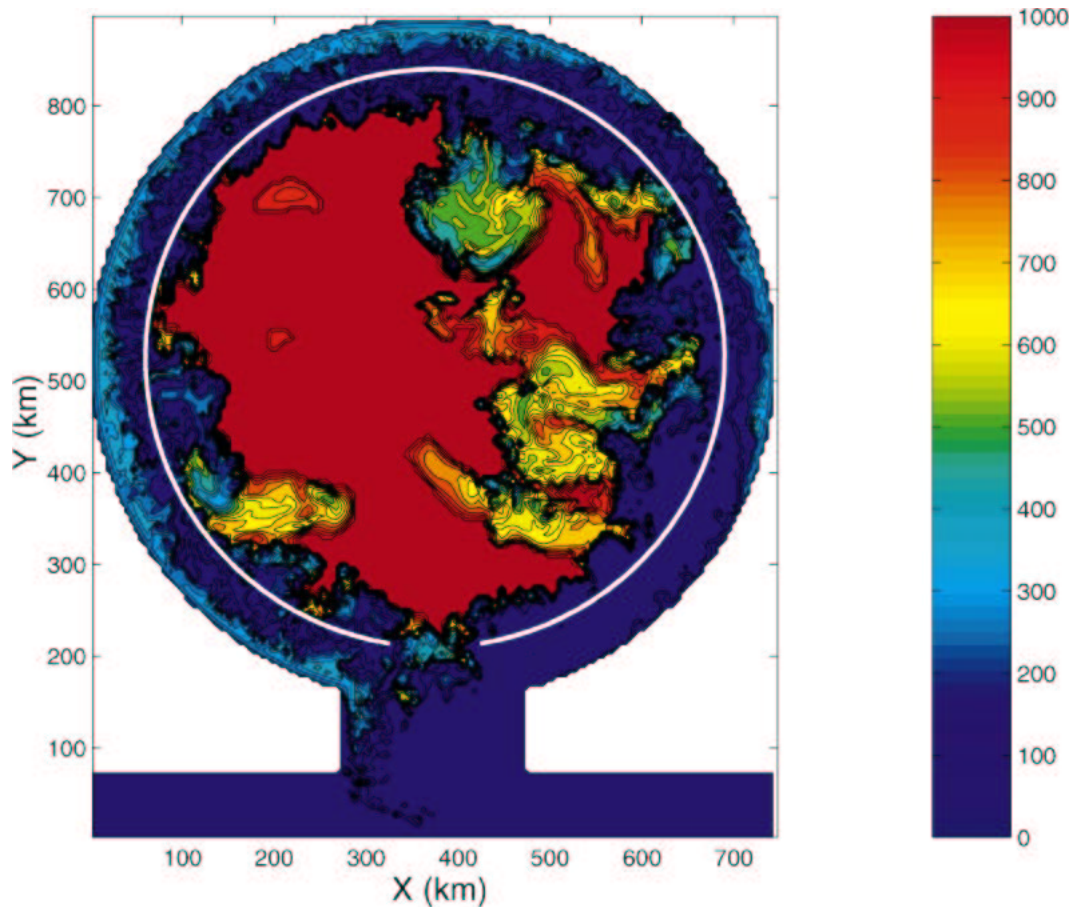The balances averaged in the azimuthal direction at

FIG. 7. Mixed layer depth (m) at the end of the cooling period in year 22; contour interval = 100 m.

150-m depth, calculated over the final 5 years of integration, are shown in Fig. 9 as a function of radius. The shaded area indicates the region of sloping topography. Mean advection acts to warm the region over the sloping bottom as a result of the cyclonic rim current carrying warm, open ocean water into the marginal sea. This warming is balanced primarily by convection due to heat loss to the atmosphere, and lateral eddy fluxes. Horizontal diffusion acts to spread the boundary current laterally by cooling the warmest waters near the outer boundary and warming the seaward region of the boundary current, but it has very little direct effect on the heat balance outside the boundary current. Eddy fluxes are negative over the whole slope and a maximum at the offshore edge of the boundary current. Synoptic pictures show that this is where the eddies are being formed (e.g., Figs. 6 and 8). The atmospheric cooling at this depth is largest in the center of the boundary current because convection does not penetrate as deeply here, where advection is strong, as it does in the interior, where advection is weak.

The balance in the interior is between cooling by heat loss to the atmosphere (and resulting convection) and heating due to eddy fluxes. The eddy flux divergence is essentially uniform throughout the interior. The warming due to the decay of the eddies takes place over the entire interior of the basin, far from where they were generated at the basin perimeter. In addition, the eddy flux divergence changes sign from the generation region in the boundary current into the interior, while the baroclinic shear is always cyclonic. This indicates that the eddy flux divergence is not simply related to the local mean flow, as is often assumed in eddy flux parameterization schemes. This redistribution of heat by the eddies is an inherently nonlocal process and thus cannot be properly parameterized by an eddy flux parameterization that depends only on the local mean flow characteristics. This is particularly apparent in the interior where the mean flow is driven by the eddies, not the other way around as it is in the boundary current.

The vertical transport $\int w\, ds$, where s is the along-boundary coordinate, averaged over the last 5 years of integration, is shown in Fig. 10. Mean vertical motions everywhere within the interior are small. The downwelling is concentrated in two areas within the boundary current. The dominant downwelling is found along the boundary and sloping bottom. This is similar to the downwelling boundary layer discussed by Spall (2003),
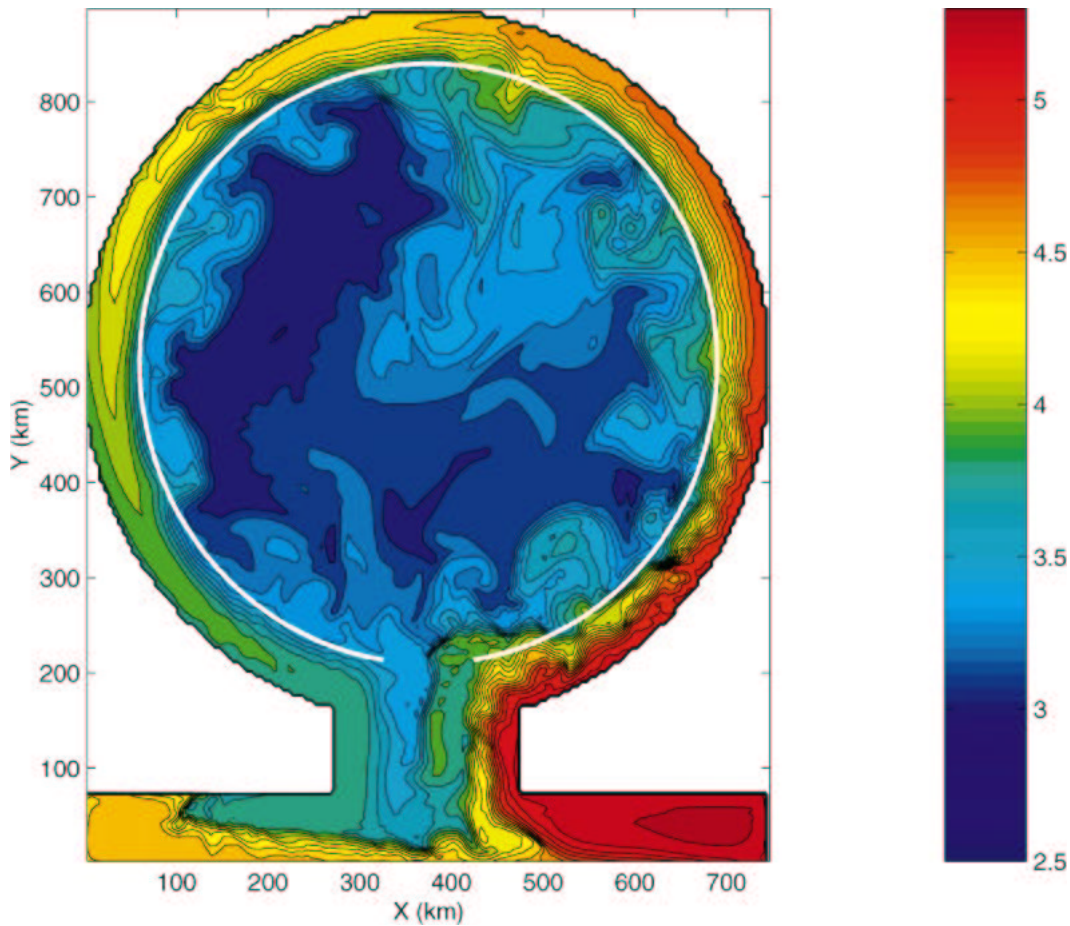
FIG. 8. Upper-level temperature (°C) at the end of month 4 in year 22; contour interval = 0.1.

Pedlosky (2003), and Barcilon and Pedlosky (1967) for cases in which the wall is vertical. They used linear, analytic models to show that horizontal mixing of density near the boundary is balanced by vertical advection. In the present model that is connected to the open ocean, the advection is due to both horizontal and vertical components and mixing is due to both explicitly resolved eddy fluxes and parameterized horizontal diffusion. The vertical velocity that advects warm water downward to balance the diffusive cooling results in stretching in the
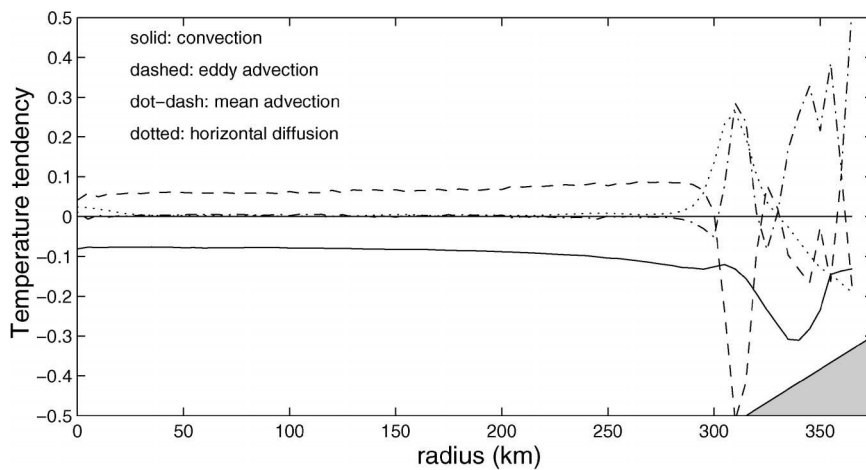

FIG. 9. Azimuthally averaged terms in the temperature equation (10^{-7} °C s^{-1}).

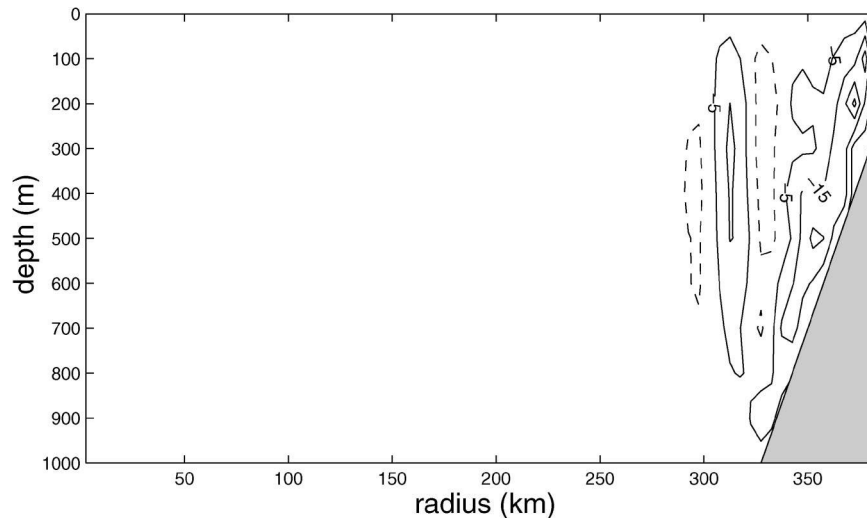FIG. 10. Azimuthally integrated vertical velocity as a function of radius (contour interval = 10 m² s⁻¹; solid contours downward).

vorticity equation. This stretching is balanced by lateral diffusion of vorticity into the solid boundary, which is why the near-boundary region is the preferred site for downwelling. Although such a simple analytic solution is not possible for the present case of a sloping bottom, the location and scale of this boundary layer, and its continuity with the downwelling along the vertical section of the wall, suggest that its dynamics are analogous to that found in the flat-bottom cases. The downwelling can also be inferred from the cooling of the temperature along the boundary, as discussed by Spall and Pickart (2001).

There is also a second site of downwelling located on the offshore edge of the boundary current. This downwelling is located where the eddies that carry heat into the basin interior are formed and the eddy flux divergence is strongly cooling the boundary current. This balance between lateral eddy flux divergence and vertical advection of the mean stratification is expected from quasigeostrophic wave–mean flow interaction theory (Pedlosky 1979, 371–377). The vertical advection carries warm water downward and so tends to warm the water column and balance the eddy flux divergence.

The net downwelling in the interior of the basin is negligible at all depths, so there is no mean baroclinic overturning circulation that connects the near-boundary region to the interior of the basin. The exchange of heat and momentum is carried entirely by the eddies that originate in the boundary current and die in the basin interior. This important role of eddy fluxes from the boundary current into the interior is consistent with the observational studies of Lilly et al. (1999, 2003) and SJPO, the former of which clearly show the formation of eddies from the Irminger Current along west Greenland that transport boundary current water into the in-

terior of the Labrador Sea, resulting in restratification of the wintertime deep convection sites.

4. Theory and integral constraints

In this section, basic integral constraints on the mass and heat balances within the marginal sea are used to derive estimates of the water mass properties and characteristics of the circulation within the marginal sea as a function of the basic parameters of the system. The approach is very idealized and is intended to provide general insight into how the bulk properties of the thermohaline circulation are determined. The continuous stratification of the marginal sea is represented as three distinct water masses. It is assumed that the waters flowing into the marginal sea from the open ocean have temperature T_{in}, the waters formed within the interior of the marginal sea have temperature T_0, and the waters flowing out of the marginal sea have temperature T_{out}.

a. Temperature of the interior water

The first quantity to be estimated is the temperature (or density) of the waters formed within the marginal sea relative to the temperature of the open ocean. The heat budget for the interior (flat bottom portion) of the marginal sea may be written as

$$2\pi R H_{in} \overline{u'T'} = \frac{\pi R^2 Q}{\rho_0 C_p}, \tag{3}$$

where R is the radius of the interior of the marginal sea, H_{in} is the vertical scale of the boundary current, Q is the mean surface heat flux, ρ_0 is a reference density of seawater, and C_p is the specific heat of seawater. The eddy temperature flux is represented by $\overline{u'T'}$, where u'
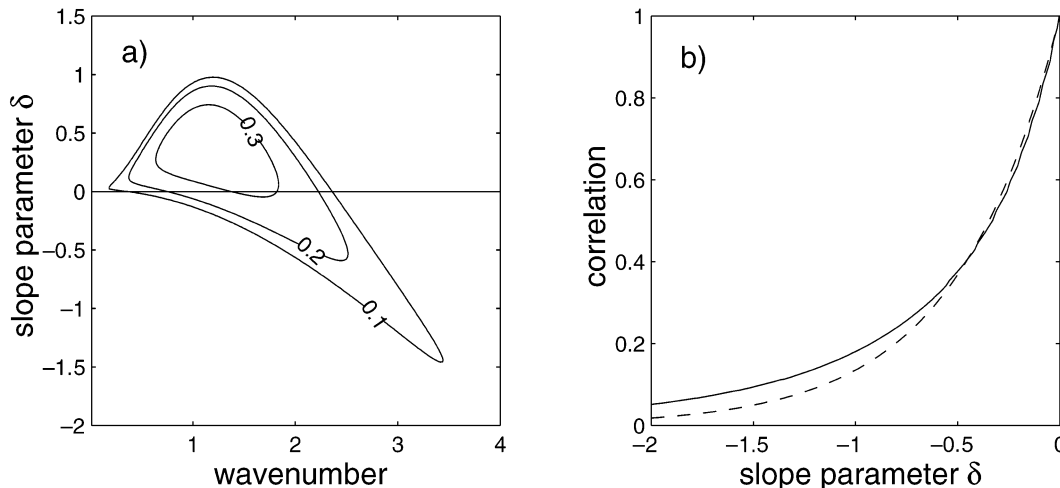
FIG. 11. (a) Growth rate of the most unstable wave as a function of wavenumber and slope parameter δ = topographic slope/isopycnal slope. (b) Correlation $\overline{u'T'}$ (solid line) and $e^{2\delta}$ (dashed line), normalized to 1 for a flat bottom ($\delta = 0$). Growth rate and solid line in (b) are from Blumsack and Gierasch (1972).

and T' are the deviations of the horizontal velocity and temperature from their time means, and the overbar indicates a temporal average. This balance assumes that the net annual heat exchange with the atmosphere is balanced by lateral eddy fluxes originating at the perimeter of the basin interior, as seen in Fig. 9. A similar balance has been used to derive the properties of localized deep convection by VMJ, Marshall and Schott (1999), and others. It is assumed that there is no mean advection through the flat interior of the basin. This is reasonable for the flat bottom f-plane calculations considered here. Calculations in which the Coriolis parameter varies with latitude give very similar results, so this analysis is relevant to the more general case as well.

The source of the eddies is the boundary current that flows over the sloping bottom. Here the general approach of VMJ and Stone (1972) is followed such that the eddy heat flux is assumed to be proportional to the mean velocity V_{in} and temperature anomaly of the boundary current $(T_{in} - T_0)$ as

$$\overline{u'T'} = cV_{in}(T_{in} - T_0), \qquad (4)$$

where c is a nondimensional correlation coefficient. VMJ and Spall and Chapman (1998) empirically found $c \approx 0.025$ over a wide range of flat-bottom cases based on laboratory and numerical model experiments. The temperature anomaly $T_{in} - T_0$ is the temperature change across the boundary current and so represents the density of the water formed in the interior of the marginal sea relative to the open-ocean temperature.

The present case differs from those considered by Stone (1972), VMJ, Visbeck et al. (1997), and Spall and Chapman (1998) because the baroclinic flow resides over topography. Blumsack and Gierasch (1972) present a simple quasigeostrophic stability analysis for a baroclinic flow over a sloping bottom (see also the recent study SGAFD). Their solution for growth rate η_i as a

function of wavenumber μ (nondimensionalized by the internal deformation radius) and bottom slope parameter δ, which is the ratio of the bottom slope to the isopycnal slope, may be written as

$$\eta_i = \left\{ \frac{\mu - \tanh(\mu)}{\tanh(\mu)}(1 - \delta) - \frac{1}{4}\left[\frac{\delta}{\tanh(\mu)} - \mu\right]^2 \right\}^{1/2}, \quad (5)$$

and is shown in Fig. 11a. The flat-bottom case is given by $\delta = 0$. The present situation of a warm boundary current flowing cyclonically around a deep basin has $\delta < 0$ (see Fig. 4a). The growth rate decreases with increasingly negative δ. The wavenumber of the maximum unstable wave also increases, indicating that the most unstable waves decrease in scale. As the bottom slope increases, it becomes increasingly more difficult for parcels to move across the topography. Bottom slopes greater than about -1.5 times the isopycnal slope essentially stabilize the flow. Currents with the topography parallel to or steeper than the isopycnals ($\delta > 1$) are also stabilized. This is generally the case for deep western boundary currents. The boundary current structure found in the central calculation (Fig. 4) has $\delta \approx -1$, typical of boundary currents in the Labrador Sea.

The linear theory of Blumsack and Gierasch (1972) also provides an estimate of the eddy heat flux as a function of the bottom slope parameter, growth rate, and mean flow, which may be written

$$\overline{u'T'} \propto \frac{\tanh(\mu)}{\mu - \tanh(\mu)} \eta_i V_{in}(T_{in} - T_0). \qquad (6)$$

The linear theory does not provide the constant of proportionality but does give its dependence on δ (through the relationship to η_i and μ plotted in Fig. 11a). The ratio of $\overline{u'T'}$ to $V_{in}(T_{in} - T_0)$, given by (6), is shown in Fig. 11b as a function of the bottom slope parameter δ for the most unstable wave. The value has been ar-

bitrarily set to 1 for a flat bottom. The eddy heat flux is greatly reduced as the bottom slope increases relative to the isopycnal slope. For typical values of $\delta = O(-1)$, the eddy heat flux is less than 20% of what would be expected for the same strength of baroclinic flow over a flat bottom. The growth rate η_i also decreases with increasingly negative δ, as seen in Fig. 11a, but it does not decrease as rapidly as the eddy flux. This indicates that the decrease in eddy flux with increasing bottom slope is due both to a decrease in the growth rate of the unstable waves and a decrease in the correlation between the perturbation velocity and the perturbation temperature. The eddy heat flux for $\delta < 0$ can be closely approximated by the exponential $e^{2\delta}$, as shown by the dashed line. This simple exponential estimate of the eddy heat flux will be used to close the heat budget (4).

Much work has been done testing balances similar to (4) for a flat bottom, which is just a special case with $\delta = 0$. In these studies, the relationship between the eddy heat flux and the mean flow parameters is remarkably constant such that $c \approx 0.025$ over a wide range of applications (VMJ; Visbeck et al. 1997; Marshall and Schott 1999). This empirical finding is also consistent with a simple quasigeostrophic theory for how eddies self-propagate, which gives the same scaling but directly estimates an upper bound of $c \approx 0.045$ (Spall and Chapman 1998). Combining this understanding of the flat-bottom behavior with the theory for the sloping bottom, $c = 0.025 \, e^{2\delta}$, and thus the eddy heat flux is parameterized as

$$\overline{u'T'} = 0.025 e^{2\delta} V_{in}(T_{in} - T_0). \quad (7)$$

The velocity of the boundary current V_{in} is related to the temperature anomaly of the boundary current through the thermal wind relation:

$$V_{in} = \frac{\alpha g (T_{in} - T_0) H_{in}}{\rho_0 f_0 L}, \quad (8)$$

where L is the width of the sloping topography. The vertical scale H_{in} is the depth of the inflowing water, taken to be the average depth of the water over the sloping bottom.

An estimate of the equilibrium temperature of the dense water in the basin interior is found by combining (3), (7), and (8) to give

$$(T_{in} - T_0) = \frac{1}{H_{in}} \left(\frac{R f_0 L Q}{2 \alpha g C_p c} \right)^{1/2}. \quad (9)$$

This result differs significantly from the analogous scaling for isolated deep convection derived by VMJ. Its power dependence on the surface buoyancy forcing and the radius of the basin are different, but more important is that this scaling is also dependent on the rotation rate f_0, the width of the topography L, and the slope of the bottom (through c). This scaling has the same parameter dependence as the scaling of Chapman (1998), who allowed for a finite-width region over which the cooling

decreased to zero. This width in his scaling is replaced by the width of the topography L in the present case, but leads to the same result. The scaling of VMJ is reproduced if the width of the topography is replaced by the internal deformation radius. The width of the topographic slope is, in general, much wider than the deformation radius at high latitudes, and so the present scaling is more appropriate for eddy fluxes driven by instability of the boundary current. This is true even if the scale of the eddies is on the order of the deformation radius (as is expected from linear instability theory). It is the width of the slope that determines the baroclinic shear of the mean boundary current, which in turn influences the eddy heat flux.

A series of numerical model calculations have been carried out in which the basin radius, surface heat flux, Coriolis parameter, width and amplitude of the topographic slope, and depth of the basin have been varied, as summarized in Table 1. For computational efficiency, the diameter of the marginal sea has been decreased to 500 km for most of these sensitivity studies. The general properties of the circulation in all of these calculations (except for the flat bottom, as discussed further below) are the same as for the central case discussed earlier. For comparison with the theory, the vertical scale height H_{in} was taken to be one-half the depth of the basin, consistent with the average depth of the inflowing warm water. The slope parameter δ was taken to be -0.8 for all cases in which the bottom depth on the boundary was 20% of the basin depth (200 m for the standard 1000-m-deep basin). This is based on the finding that the isopycnals intersect the bottom at about the midpoint of the slope and outcrop on the offshore side of the topography. For the cases in which the bottom depth on the boundary was 600 and 800 m (runs 4 and 5), assuming that the isopycnals slope from the midpoint of the topography to the surface on the offshore side of the front, $\delta = -0.4$ and -0.2, respectively. The results are not overly sensitive to how δ is defined as long as it is consistent with the mean shear found in the model.

The density of the interior waters formed in the marginal sea, relative to the mean temperature of the inflowing water, was calculated for each of the runs and is compared to the theoretical estimate (9) in Fig. 12a. The central case is indicated by the asterisk at $(T_{in} - T_0) = 1.15°C$. The temperature anomaly of the waters formed in the marginal sea varies from approximately 0.5° to over 2°C for all of the calculations. There is very close agreement between the theory and the model results, with a correlation of 0.95 and a least squares fit slope of 1.23. The density of the waters formed in the interior of the basin varies by a large amount, even for the same heat loss over the marginal sea. The controlling factor is the effectiveness of the instability process in transporting the warm waters from the boundary current into the basin interior.

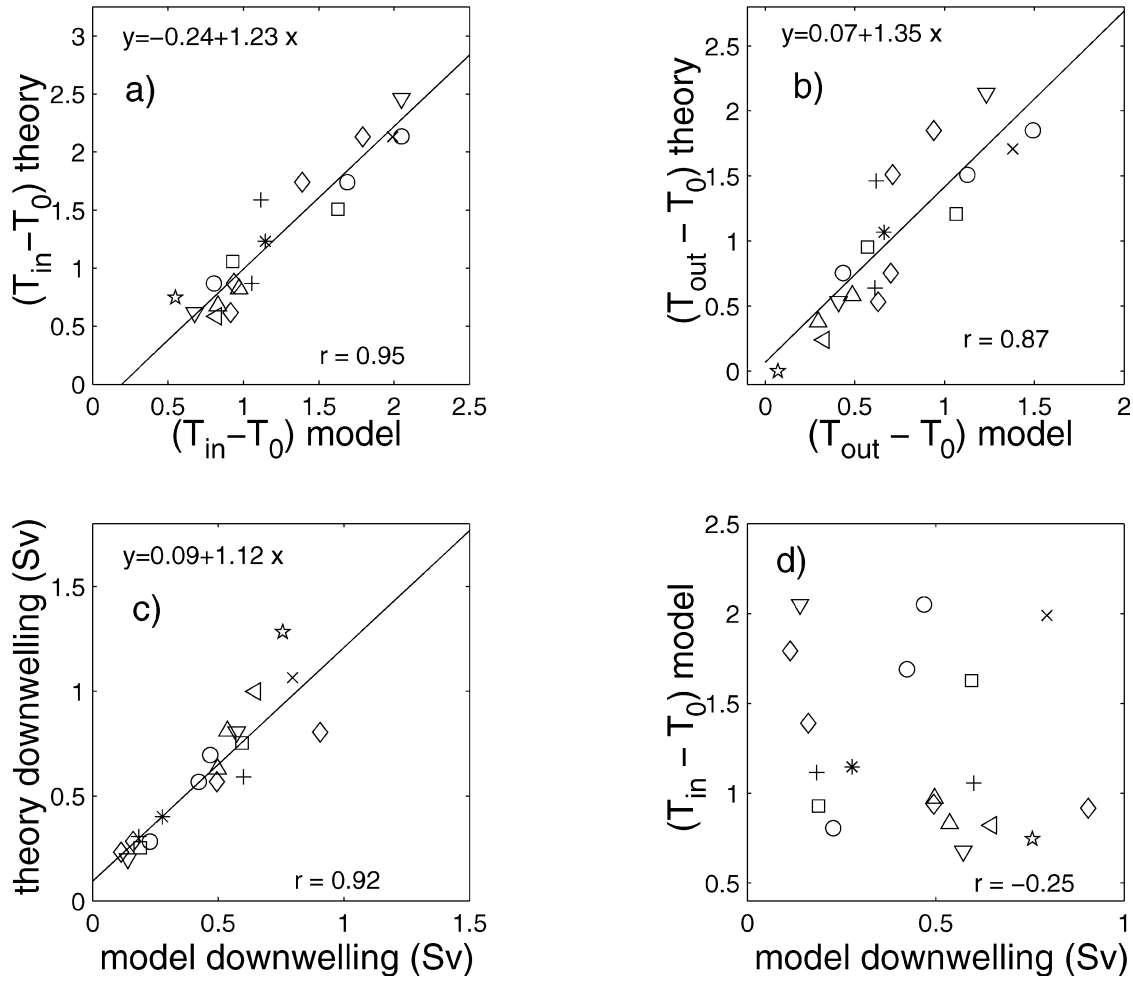The flat-bottom calculation, indicated by the star, re-

FIG. 12. Comparison between the theory and the series of numerical model calculations summarized in Table 1: (a) temperature anomaly of waters formed in the interior $T_{in} - T_0$ (°C), (b) temperature anomaly of outflowing waters $T_{out} - T_0$ (°C), (c) downwelling in the basin (10^6 m^3 s^{-1}), and (d) comparison between downwelling and interior temperature anomaly. Correlation coefficients are given in the lower right of each panel and a least squares fit line to the points is given in the upper part of (a)–(c).

quires special treatment and will be discussed after the analysis of the sloping bottom cases.

b. Temperature of the outflowing water

The waters flowing out of the marginal sea are, in general, cooler than the inflowing waters, as required to balance the heat budget in the marginal sea. However, the outflowing waters can be much warmer than the coldest waters formed in the interior of the basin. The average temperature of the outflowing waters can be estimated by requiring that the net heat flux into the marginal sea through the boundary current balances the net heat loss to the atmosphere and that the net mass flux into the marginal sea be zero. The heat budget may be written as

$$T_{in}V_{in}H_{in}L - T_{out}V_{out}H_{out}L = \frac{\pi R^2 Q}{\rho_0 C_p}, \quad (10)$$

where the subscripts "in" and "out" refer to the properties of the inflowing and outflowing boundary currents.

The inflowing heat transport can be written, by making use of (8) and (9), as

$$T_{in}V_{in}H_{in}L = \frac{RQL}{2\rho_0 C_p c}. \quad (11)$$

The requirement that mass be balanced within the marginal sea requires that $V_{in}H_{in}L = V_{out}H_{out}L$. This may be combined with (10) and (11) to obtain an expression for the temperature anomaly of the outflowing water, relative to the temperature of the cold waters formed in the interior of the basin, as

$$T_{out} - T_0 = (T_{in} - T_0)(1 - 2\pi Rc/L)$$

$$= (T_{in} - T_0)(1 - \epsilon). \quad (12)$$

The factor $\epsilon = 2\pi Rc/L$ may be interpreted as the fraction

of the inflowing waters that are fluxed into the interior by eddies. For the standard configuration, $\epsilon = 0.13$. For strongly sloping topography (c $\ll$ 1), small basins, or wide topographic slopes, the outflowing water is close to the temperature of the inflowing water. The density of the outflowing water increases as the basin size increases, the width of the topographic slope decreases, or as the topographic slope itself decreases (c increases). The implication is that the transport in the boundary current, and the exchange between the marginal sea and the open ocean, is enhanced as ϵ decreases. As a reference, ϵ for the Labrador Sea is approximately 0.1.

The average temperature of the outflowing waters was calculated from the series of model calculations and is compared to the theoretical estimate (12), making use of (9), in Fig. 12b. Once again there is general agreement between the model and theory, although the comparison is not as close as it was for $T_{in} - T_0$. This is not surprising since the theory for the outflowing temperature uses the theory for $(T_{in} - T_0)$ as part of the solution. In particular, the theory predicts that the outflowing temperature should increase with increasing f_0 but the model results in much less variation with f_0. The theory also predicts an increase with increasing L, largely due to an increase in $T_{in} - T_0$, but both the inflowing and outflowing temperature anomaly show little dependence on the slope width. Nonetheless, the general tendency is well predicted by the theory, and the correlation remains high: $r = 0.87$.

c. Downwelling in the marginal sea

The requirement that the net cooling in the marginal sea be balanced by advection through the strait does not immediately reveal the means by which the heat balance is satisfied. The outflowing colder water could be in the upper water column, in which case the heat transport would be carried primarily by a horizontal gyre. The dense waters could also flow out of the marginal sea at a depth much greater than the inflowing waters, indicating that the heat transport is achieved by an overturning, or sinking, circulation. The distinction between these two heat transport mechanisms is significant, as the sea surface temperature can be much colder for the case in which the heat transport is carried by the horizontal gyre rather than the overturning gyre, as demonstrated by Spall and Pickart (2001).

The maximum mean downwelling in the marginal sea can be estimated by considering the thickness of the outflowing water H_{out} in comparison with that of the inflowing water H_{in}. The net downwelling transport W is given simply by this change in thickness times the width of the outflowing boundary current L and the velocity of the outflowing boundary current V_{out}:

$$W = (H_{out} - H_{in})LV_{out}. \tag{13}$$

Mass conservation in the marginal sea, and the use

of (12) and thermal wind, allows the thickness of the outflowing waters to be written as

$$H_{out} = \frac{V_{in}H_{in}}{V_{out}} = \frac{H_{in}}{(1 - \epsilon)^{1/2}}. \tag{14}$$

For $\epsilon = O(0.1)$, the change in thickness between the inflowing boundary current and the outflowing boundary current is only $O(5\%)$, and so would be difficult to observe directly, in either the model or observations.

The downwelling W may now be derived:

$$W = \frac{H_{in}}{\rho_0}\left(\frac{RLQ\alpha g}{2C_p cf_0}\right)^{1/2}[1 - (1 - \epsilon)^{1/2}]$$

$$= [1 - (1 - \epsilon)^{1/2}]V_{in}H_{in}L. \tag{15}$$

The downwelling within the marginal sea is simply related to the inflowing transport $V_{in}H_{in}L$ by a factor of $1 - (1 - \epsilon)^{1/2}$. As eddies flux all of the inflowing boundary current water into the interior, $\epsilon \to 1$, and all of the inflowing boundary current water downwells within the marginal sea. For small ϵ (steep slopes, small basins, or wide topographic slopes), only a small fraction of the inflowing transport downwells within the basin. This is made clear by considering the limit of $\epsilon \ll 1$, in which case (15) may be approximated as

$$W \approx \frac{\epsilon}{2}V_{in}H_{in}L. \tag{16}$$

The maximum downwelling within the marginal sea has been calculated for each of the model calculations and is compared to the theory in Fig. 12c (correlation 0.92). The downwelling rate varies by almost an order of magnitude even for those calculations with the same surface heat flux. The downwelling rate increases with increasing transport in the boundary current, which results in these calculations mainly from increasing the inflowing velocity or the basin depth. The inflowing velocity, in turn, is determined by the density of the water in the interior of the basin, $T_{in} - T_0$, and the thermal wind relation. Because the thermal wind results in larger velocities for the same temperature gradient at lower latitudes, the downwelling increases with decreasing latitude. The downwelling also increases with increasing ϵ, which results primarily from decreasing the bottom slope or increasing the radius of the basin. The ability of the bottom slope to stabilize the boundary current influences not only the density of the waters formed in the interior of the basin, but also the total amount of downwelling found within the marginal sea. The theory and model demonstrate the somewhat counterintuitive result that increasing the bottom slope results in more dense waters in the interior of the marginal sea, but less total downwelling within the marginal sea.

This result indicates that the downwelling rate is not simply related to the amount of cooling or the density of the water masses formed. This is clear from Fig. 12d in which the downwelling rate is plotted against the

density anomaly of the waters formed in the interior of the marginal sea. The two properties have a weak, negative correlation.

d. Heat transport

The mechanism of heat transport within the marginal sea is also of interest. For some marginal seas, such as the Mediterranean Sea, the heat transport is carried primarily by an overturning gyre, where light water enters the basin in the upper ocean and dense water leaves the basin in the deep ocean. In other basins, such as the Labrador Sea, the horizontal circulation appears to also be an important heat transport mechanism, where the water simply becomes more dense as it encircles the basin with little net downwelling (Spall and Pickart 2001). Understanding the dynamical reasons for these differences is important to understanding the differences in the thermohaline circulation in a variety of marginal seas.

The ratio of the heat transport by the horizontal gyre to the heat transport by the overturning gyre can be estimated from the basic properties derived thus far. It is important to note that the downwelling takes place near the boundary, and so the heat flux carried by the overturning gyre is proportional to the temperature difference of the inflowing water and the outflowing water, $T_{in} - T_{out}$. Making use of the theoretical estimate for W, the ratio of horizontal to overturning heat transport can be estimated as

$$\frac{V_{in} H_{in} L(T_{in} - T_{out})}{W(T_{in} - T_{out})} = \frac{1}{1 - (1 - \epsilon)^{1/2}} \approx \frac{2}{\epsilon} \gg 1. \quad (17)$$

The final approximation makes use of $(1 - \epsilon)^{1/2} \approx 1 - \epsilon/2$ for $\epsilon \ll 1$. The relative importance of the horizontal and overturning gyres depends only on the parameter ϵ. In the limit of weak eddy fluxes from the boundary current ($\epsilon \ll 1$), the horizontal gyre transports much more heat than the overturning gyre. For large basins or strong eddy fluxes, $\epsilon \to 1$, the final approximation in (17) is not valid, and the heat transport is equally divided between the horizontal and overturning gyres. These estimates are consistent with the findings in high-resolution numerical models that the horizontal gyre transports more than one-half of the total meridional heat transport at high latitudes in the North Atlantic Ocean (Böning and Bryan 1996).

e. Flat-bottom theory

The flat (or very weakly sloping topography such that $\epsilon \geq 1$) case requires special consideration. The heat budget (3) that was used to calculate the temperature of waters formed within the marginal sea assumed that the eddy flux takes place all along the perimeter of the marginal sea. If the eddy fluxes are strong enough or the marginal sea is large enough, then the heat carried into the marginal sea in the boundary current will be fluxed into the interior by eddies before the boundary current has extended around the marginal sea. This is what happens for a 500-km diameter basin with a flat bottom, as indicated by the mean upper-level temperature shown in Fig. 13. In this case, the eddy contribution will be nonzero only over the portion of the boundary where the boundary current exists.

The distance s that the boundary current will penetrate into the marginal sea is determined by the distance it takes for the eddy flux to balance the advective heat flux into the marginal sea:

$$\overline{su'T'} = L_{flat} U_{flat}(T_{in} - T_0)_{flat}. \quad (18)$$

The length scale L, velocity, and temperature anomaly of the boundary current now have the subscript "flat" because these will, in general, be different from the previous results for sloping topography near the boundary. Making use of the eddy flux parameterization (4), the distance s is simply

$$s = \frac{L_{flat}}{c}, \quad (19)$$

where L_{flat} is the width of the boundary current. The flat bottom theory of Spall (2003) shows that the width of the boundary current in this case scales approximately as the internal deformation radius. For the open-ocean stratification used here, the internal deformation radius is 17 km. Equation (19) then predicts that the boundary current over a flat bottom, with $c = 0.025$, would be eroded in 680 km. This is 43% of the perimeter of the 500-km diameter marginal sea and is consistent with the penetration found in Fig. 13. For $\epsilon = 1$, the distance over which the boundary current is eroded exactly matches the perimeter of the basin. The results derived here are applicable when the parameter $\epsilon \geq 1$.

The interior heat budget may then be used to estimate the temperature of the water in the interior as

$$(T_{in} - T_0)_{flat} = \frac{1}{H_{in}} \left(\frac{\pi R^2 Qf}{\alpha g C_p} \right)^{1/2}. \quad (20)$$

The temperature in the interior for the flat bottom has the same parameter dependence as the sloping cases for the heat flux and Coriolis parameter, but now depends linearly on the radius of the basin. It is independent of the eddy flux parameter c and the width of the slope L, which in effect control the strength of the eddy flux. In general, the temperature anomaly for the flat or weakly sloping bottom cases will be less than it is for basins with a steep slope near the boundaries because all of the boundary current heat transport in the flat bottom case goes toward balancing the surface heat loss. The temperature anomaly for the flat bottom is simply related to the temperature anomaly for the sloping bottom by the parameter ϵ as

$$(T_{in} - T_0)_{flat} = \epsilon^{1/2}(T_{in} - T_0). \quad (21)$$

The downwelling within the marginal sea for the flat-
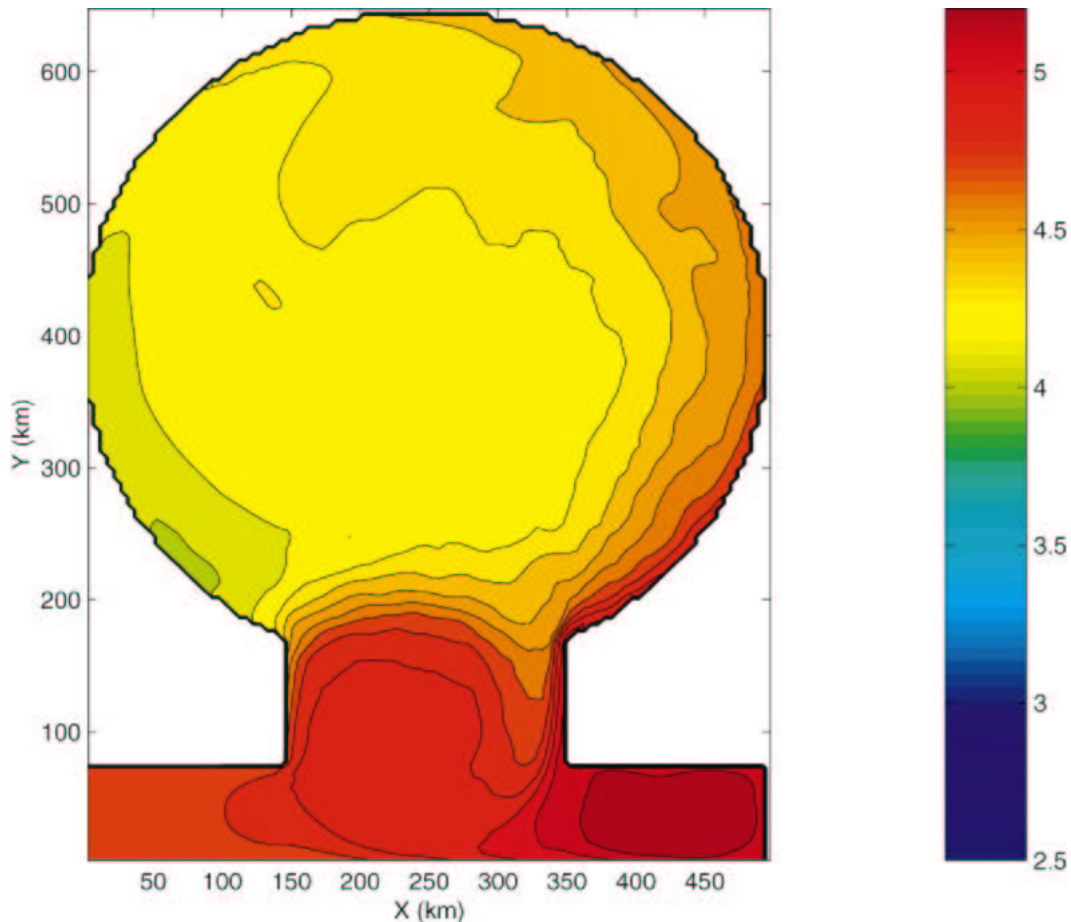
FIG. 13. Mean upper-level temperature (°C) for the flat-bottom calculation; contour interval = 0.1.

bottom case is the same as the transport into the marginal sea because the boundary current is entirely eroded by eddy fluxes before it can exit the basin. In this case, the downwelling is

$$W_{\mathrm{flat}} = V_{\mathrm{in}} H_{\mathrm{in}} L_{\mathrm{flat}} = \frac{H_{\mathrm{in}}}{\rho_0} \left(\frac{\alpha g \pi R^2 Q}{f_0 C_p} \right)^{1/2}. \quad (22)$$

Expressions (20) and (22) were used for the stars in Fig. 12. The theory also predicts that the outflowing dense waters will have the same temperature as the waters formed in the interior of the marginal sea ($T_{\mathrm{out}} - T_0 = 0$), which is close to what is found in the model (Fig. 12b). In this case the dense waters flow out of the marginal sea as bottom-trapped currents along both the left- and right-hand sides of the strait, as in Spall (2003).

5. Summary and conclusions

Basin-scale heat budgets and linear stability theory have been used to provide theoretical estimates of the properties of the watermass transformation and thermohaline circulation in marginal seas subject to buoyancy loss at the surface. Specific quantities of interest

include the density of waters formed in a marginal sea, the density of the outflowing waters, the strength of the boundary currents that encircle the marginal sea, the magnitude of downwelling within the marginal sea, and the mechanisms of heat transport. The theory compares well to results from a high-resolution primitive equation model over a wide range of parameter space.

Although the general approach taken here is similar to what has been used to characterize localized open-ocean convection (e.g., Visbeck et al. 1996), the inclusion of boundaries and an open ocean allows for equilibrium solutions and a full three-dimensional thermohaline circulation. The heat loss in the marginal sea is ultimately balanced by lateral advection in boundary currents from the open ocean. The strength of the boundary current is determined as part of the solution. Boundaries also support the downwelling component of the thermohaline circulation. The downwelling is located within a narrow boundary layer over the sloping bottom and along the offshore edge of the boundary current, and is not directly related to the density of waters formed in the interior of the marginal sea. The downwelling within the boundary layer is analogous to the boundary

layers over a flat bottom discussed previously by Barcilon and Pedlosky (1967), Spall (2003), and Pedlosky (2003). The downwelling on the offshore side of the front is required to balance the eddy heat flux divergence that supplies the interior of the basin with warm water.

The key process that determines the properties of the watermass transformation and thermohaline circulation in the marginal sea is the interaction between the cyclonic rim current along the basin perimeter and the interior of the marginal sea. This exchange is controlled by baroclinic instabilities of the boundary current that, for realistic configurations, are on scales somewhat smaller than the internal deformation radius. The ratio of the isopycnal slope to the bottom slope is the fundamental parameter that quantifies this exchange. For even moderately steep topography, the eddy fluxes resulting from surface-intensified fronts are much weaker than would be expected for the analogous flat-bottom theory. Most marginal seas are in such a topographically controlled state. Bottom-trapped currents, such as deep western boundary currents, can be completely stabilized by the topography. The theory presented here provides a simple modification of the flat-bottom parameterization of eddy fluxes due to baroclinic instability that accounts for such topographic effects. However, it is also evident that the seasonal restratification of the marginal sea interior is due to nonlocal sources of eddies and is thus very difficult to represent using any local parameterization scheme.

REFERENCES

Barcilon, V., and J. Pedlosky, 1967: A unified linear theory of homogeneous and stratified rotating fluids. *J. Fluid Mech.,* **29,** 609–621.

Blumsack, S. L., and P. J. Gierasch, 1972: Mars: The effects of topography on baroclinic instability. *J. Atmos. Sci.,* **29,** 1081–1089.

Böning, C. W., and F. O. Bryan, 1996: Large-scale transport processes in high-resolution circulation models. *The Warmwatersphere of the North Atlantic Ocean,* W. Krauss, Ed., Gebrüder Borntraeger, 91–128.

Bryan, F. O., 1987: Parameter sensitivity of primitive equation ocean general circulation models. *J. Phys. Oceanogr.,* **17,** 970–985.

Chapman, D. C., 1998: Setting the scales of the ocean response to isolated convection. *J. Phys. Oceanogr.,* **28,** 606–620.

Katsman, C. A., M. A. Spall, and R. S. Pickart, 2004: Boundary current eddies and their role in the restratification of the Labrador Sea. *J. Phys. Oceanogr.,* in press.

Lilly, J. M., P. B. Rhines, M. Visbeck, R. E. Davis, J. R. N. Lazier, F. Schott, and D. Farmer, 1999: Observing deep convection in the Labrador Sea during winter 1994–95. *J. Phys. Oceanogr.,* **29,** 2065–2098.

——, ——, F. Schott, K. Lavender, J. Lazier, U. Send, and E. d'Asaro, 2003: Observations of the Labrador Sea eddy field. *Progress in Oceanography,* Vol. 59, Pergamon, 75–176.

Marshall, J., and F. Schott, 1999: Open-ocean convection: Observations, theory, and models. *Rev. Geophys.,* **37,** 1–64.

——, C. Hill, L. Perelman, and A. Adcroft, 1997: Hydrostatic, quasi-hydrostatic, and nonhydrostatic ocean modeling. *J. Geophys. Res.,* **102,** 5733–5752.

Mauritzen, C., 1996: Production of dense overflow waters feeding the North Atlantic across the Greenland–Scotland Ridge. Part 1: Evidence for a revised circulation scheme. *Deep-Sea Res.,* **43,** 769–806.

Park, Y.-G., and J. A. Whitehead, 1999: Rotating convection driven by differential bottom heating. *J. Phys. Oceanogr.,* **29,** 1208–1220.

——, and K. Bryan, 2000: Comparison of thermally driven circulations from a depth-coordinate model and an isopycnal-layer model. Part I: Scaling-law sensitivity to vertical diffusivity. *J. Phys. Oceanogr.,* **30,** 590–605.

Pedlosky, J., 1979: *Geophysical Fluid Dynamics.* Springer-Verlag, 624 pp.

——, 2003: Thermally driven circulations in small ocean basins. *J. Phys. Oceanogr.,* **33,** 2333–2340.

Spall, M. A., 2003: On the thermohaline circulation in flat bottom marginal seas. *J. Mar. Res.,* **61,** 1–25.

——, and D. C. Chapman, 1998: On the efficiency of baroclinic eddy heat transport across narrow fronts. *J. Phys. Oceanogr.,* **28,** 2275–2287.

——, and R. S. Pickart, 2001: Where does dense water sink? A subpolar gyre example. *J. Phys. Oceanogr.,* **31,** 810–826.

Stone, P., 1972: A simplified radiative–dynamical model for the static stability of rotating atmospheres. *J. Atmos. Sci.,* **29,** 405–418.

Visbeck, M., J. Marshall, and H. Jones, 1996: Dynamics of isolated convective regions in the ocean. *J. Phys. Oceanogr.,* **26,** 1721–1734.

——, ——, T. Haine, and M. Spall, 1997: Specification of eddy transfer coefficients in coarse-resolution ocean circulation models. *J. Phys. Oceanogr.,* **27,** 381–402.